



Rapid transition of sediment consolidation across an expanding mangrove fringe in the Firth of Thames New Zealand

Robert R. Roskoden¹ · Karin R. Bryan² · Isabel Schreiber¹ · Achim Kopf¹

Received: 19 February 2019 / Accepted: 27 August 2019 / Published online: 15 October 2019
© Springer-Verlag GmbH Germany, part of Springer Nature 2019

Abstract

Mangrove habitats are complex systems, which are subjected to both natural and human external forces such as tidal variations, sediment supply, deforestation, and climate change, which in many locations are causing mangroves to decline and even disappear. Global measurements of surface elevations have been conducted at many locations to understand if sedimentation rates in mangrove areas will keep pace with sea level rise. However, extending results to other areas requires a detailed understanding of subsidence processes in mangrove areas. Here, we provide a detailed geotechnical investigation (sediment cone resistance and friction, coefficient of consolidation, grain size, normalised tip resistance and friction ratio, etc.), critical for understanding surficial sediment dynamics and vertical sediment accretion rates, of the mangrove forest edge and its surrounding mud flat in the Firth of Thames, New Zealand. Eight in situ samples were collected and tested in oedometer experiments to evaluate the coefficient of consolidation. Furthermore, a kinematic penetrometer, NIMROD, was used to estimate the resistance forces of the mud flat and mangrove forest, from which soil properties were evaluated. Our results show that mangroves are able to change soil properties to enhance sediment resistance towards erosion. An increase of sediment strength correlated with an increase of mangrove tree density as well as a decrease in the coefficient of consolidation. Hence, the increase of tree density to a decrease of the coefficient of consolidation correlates as well. In this study, our results suggest that the Firth of Thames mangroves are able to accrete enough sediment to keep up with local sea level rises if sediment supplies remain similar in the future. The correlation of tree density to the coefficient of consolidation can be used to assess future mangrove-soil interaction and mud flat progression. Finally, the applicability of literature soil classifications for the kinematic penetrometer was realized for the first time and applied to mangrove and mud flat areas.

Introduction

Mangrove forests

Mangroves occur in tropical and subtropical low-lying estuaries, river deltas, and muddy coasts and occupy 1,465,000 ha of coastline globally (Alongi 2008). Large mangrove forests in estuaries can be found, for example, in South Africa, Australia, and New Zealand (Swales et al. 2015). These coastal forests develop in mesotidal and macrotidal areas and provide a valuable habitat for flora and fauna (Alongi 2008;

Lovelock et al. 2015; Montgomery et al. 2018; Morrissey et al. 2010; Swales et al. 2015; Zhou et al. 2016). Their economic value is estimated to be around 194,000–900,000 USD per ha (Alongi 2008; Lovelock et al. 2015). Due to their specific intertidal habitat, mangrove forests are often subjected to natural hazards such as storms surges, tidal bores, cyclones, hurricanes, and tsunamis, and can play an important role in protecting low-lying coastal land (Alongi 2008; Dahdouh-Guebas et al. 2005; Kathiresan and Rajendran 2005). In addition, the reduction of hydrodynamic forces by mangrove forests promotes sedimentation and therefore land reclamation (Zhou et al. 2016).

Mangroves have been shown to keep pace with sea level rise over geologic timescales (Sasmito et al. 2016). Many studies exist investigating the modern-day mangrove sedimentation potential relative to the local sea level rise using surface elevation tables (SET) (Lovelock et al. 2015; Swales et al. 2015, 2016). Unfortunately, especially in areas where subsidence processes are important, SETs-techniques can be

✉ Robert R. Roskoden
rroskoden@marum.de

¹ MARUM–Center for Marine Environmental Sciences, University of Bremen, Leobener Straße, 28359 Bremen, Germany

² School of Science, University of Waikato, Private Bag 3105, Hamilton 3240, New Zealand

difficult to use (Alongi 2008). Shallow subsidence processes include consolidation and compaction due to the self-weight of the sediment. Consolidation is a geotechnical process in which a load (either external or self-weight) acts on the water in the pore space in between the granular soil structure, and causes the sediment to reduce its volume by dewatering. The coefficient of consolidation (c_v) describes the rate at which soil undergoes consolidation if subjected to loading. When consolidation is complete, compaction reduces its volume even further, in which case the load acts on the granular structure itself. Due to the subsidence effects, recent modelling studies show that the effect of consolidation cannot be neglected and can lead to inaccurate time estimations (up to 10 years) for wetland restoration projects (Zhou et al. 2016) and so Zhou et al. (2016) emphasise the need for in situ measurements to validate model predictions.

Detailed geotechnical information is a critical part of evaluating surficial sediment dynamics and their influence on vertical accretion rates to plan coastal engineering actions. Consolidation can be measured using a laboratory oedometer test, in which samples are subjected to a known loading. Grain size can also be measured in the laboratory but can be difficult to sample in remote areas. More efficient data sampling can be achieved with in situ cone penetration testing (*CPTu*). Consequently, to reduce the amount of sampling, further needed geotechnical parameters such as sediment strength are commonly conducted with an in situ cone penetration piezometer and later correlated to few gathered samples. However, *CPTus* have many disadvantages, such as self-weight, which complicates the logistics and is exceedingly problematic for mud flat and mangrove studies, where the intertidal nature, the soft sediments, and dense branching/root networks make boat or land access extremely difficult. Even more importantly, the self-weight often destroys the soil properties in the upper meters of the sediment (Steiner 2013).

Here, a unique kinematic free fall penetrometer called ‘NIMROD’ (Stark 2011) was chosen to investigate the geotechnical properties of a mangrove forest edge and surrounding mud flat in the Firth of Thames, New Zealand. In addition, eight in situ samples were taken and tested in oedometer experiments to evaluate the coefficient of consolidation and the grain size distribution. In our study, we explore the following scientific questions:

1. Is the coefficient of consolidation dependent on mangrove density?
2. Does the influence of mangroves distort the interpretation of the cone resistance forces for the geotechnical classification of soils?
3. Can the penetrometer resistance forces be correlated to the regional coefficients of consolidation?
4. Can this correlation shed light on how mangroves influence the consolidation process?

The answer to these research questions may help further modelling approaches for bed formation dynamics and give a clear understanding of the interaction between mangroves and the soil. Furthermore, it helps to improve future interpretation of dynamic and kinematic cone penetration investigations.

Study area Firth of Thames

The Firth of Thames, located in New Zealand’s north island (37.25° S, 175.4° E), is characterised as a ~800 km² mesotidal estuary (Fig. 1). The mangrove forest occupies an area between 1 and 1.89 m above MSL (Montgomery et al. 2018). Mean annual precipitation is ~1211 mm (Swales et al. 2015). Two rivers (Waihou and Piako) supply the Firth with 190,000 t sediment per year (Swales et al. 2015). The supplied sediment is terrigenous rhyolitic glasses, which transform into smectite muds after deposition in the Firth. The forest sits on a convex mud ramp with a gradient of approximate 0.4° to horizontal mean sea level (down-sloping seaward, Swales et al. 2015). The mangrove area is restricted to around 11 km² in the southern part of the Firth (Swales et al. 2015).

Methods

Laboratory work

Five locations (M1 to M5) were identified for push-core sampling, representing areas of differing mangrove density (Table 1). The samples were tested for their grain size distribution (for ground truthing purposes) and coefficient of consolidation. In order to test for repeatability, locations M3 to M5 (in the mangrove forest) were sampled twice with a spatial separation between replicates of up to 10 m. The first two samples were collected at the forest fringe and subsequent samples into the forest towards higher mangrove densities. Samples were taken using 25 cm long push cores. To ensure no more disturbance than necessary, samples were transported upright, keeping the in situ top/bottom position constant.

Grain size distribution was measured using the ‘Malvern Mastersizer 3000 laser diffraction particle size analyzer’. Grain size samples were taken from the middle of each core (~10 cm). The test procedure followed the pre-programmed template for marine sediment at the University Waikato. The refraction index was 1.5, particle density 1, absorption index 0.2, refractive index 1.33, and 30% ultrasound for the pre-measurement organic matter which was not dissolved beforehand.

A one-dimensional compression test, called the oedometer test, measures the compaction of a soil due to vertical loading, which results in dewatering. The specimen is loaded incrementally, with the normal load (i.e. vertical stress) being doubled every 24 h, while vertical deformation is measured over

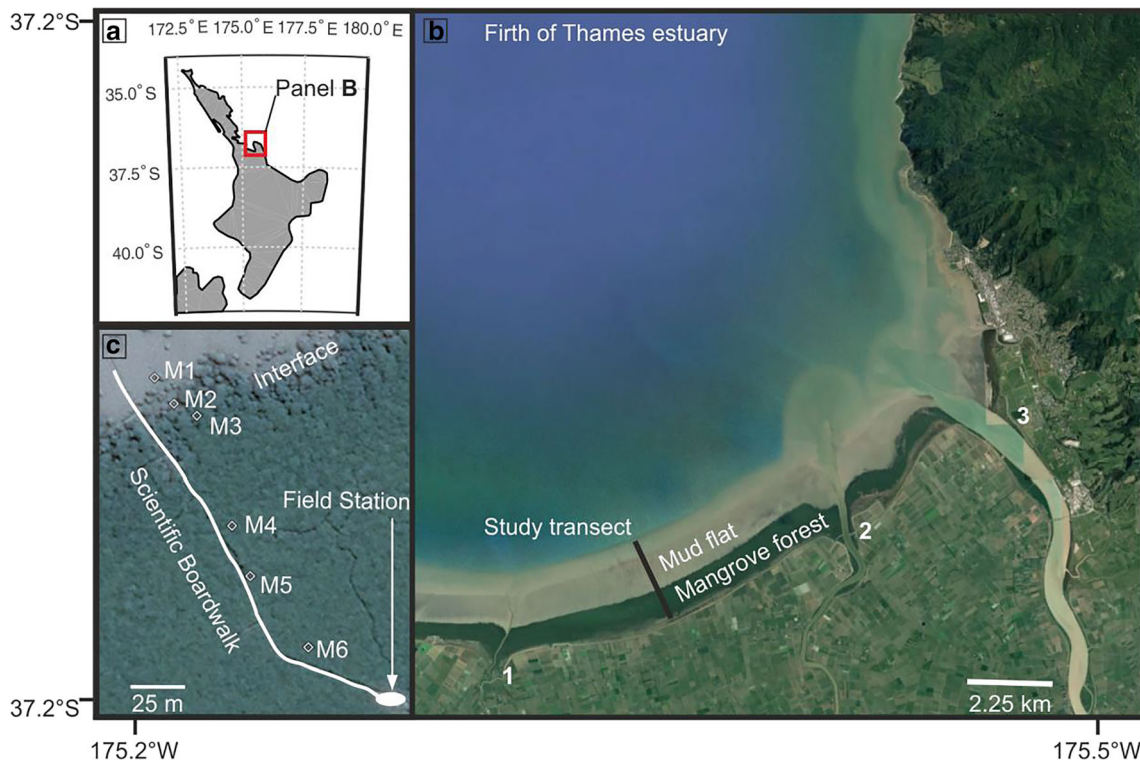


Fig. 1 (A) Matlab (version R2015a) map of the North Island of New Zealand showing the Firth of Thames in a red rectangle. (B) Modified Google Earth map (version 7.1.8.3036), Firth of Thames, New Zealand (37.25° S, 175.4° E). Marked as reference are from left to right 1 Waitakaruru River, 2 Piako River, and 3 Waihou River. The study transect (orientated perpendicular to the shoreline) is ~3.6 km east of the 1 Waitakaruru River and ~5 km west from the 2 Piako River. (C)

The study transect in the mangrove section displaying the measurement locations M1 (at the interface of ‘mud flat-mangrove forest’), M2 (behind the interface), and M3 to M6 (increasing density of mangroves). M1 to M5 also represent the sampling location for the oedometer tests. M7 to M9 (not shown in panel C) are ~800 m south of the interface ‘mud flat-mangrove forest’ and ~600 m south of M6

time. The test can characterise the following soil properties: coefficient of consolidation (c_v), compression index (C_C), recompression index (C_R), and swelling index (C_S). The test was done with the ‘Wykeham Farrance (Model 26 - WF0302)’ apparatus, following ISO 17892-5 (2017).

Since samples were taken near the surface, we assume no real vertical, in situ, total overburden effective stress on the samples. Hence, oedometer loading was sustained for 24 h at 250, 500, 1000, and 2000 g (~3–24 kPa). The log(t)-method after Casagrande and Fadum (1940) was chosen for the

Table 1 Calculated coefficient of consolidation per loading step and averaged per load and side. The table shows a gradient in coefficient of consolidations decreasing towards higher mangrove density

Location	M1	M2	M3		M4		M5			
Sample	FoT1	FoT2	FoT3	FoT4	FoT5	FoT6	FoT7	FoT8	AVG	STD
Water content										
Before	72%	63%	64%	64%	59%	59%	61%	60%	63%	4%
After	53%	52%	50%	54%	49%	49%	50%	51%	51%	2%
ρ_d [kg/m ³]	3.9E+02	5.2E+02	4.9E+02	5.4E+02	5.9E+02	6.7E+02	5.5E+02	5.3E+02	5.3E+02	7.5E+01
ρ_w [kg/m ³]	1.4E+03	1.4E+03	1.3E+03	1.5E+03	1.4E+03	1.6E+03	1.4E+03	1.3E+03	1.4E+03	8.8E+01
Void ratio										
Initial	6.36	4.47	4.84	4.27	3.86	3.27	4.18	4.39	4.5E+00	8.4E-01
Porosity	86%	82%	83%	81%	79%	77%	81%	81%	81%	3%
AVG load [cm ² /s]	1.7E-02	2.7E-03	4.2E-03	3.9E-03	3.4E-03	2.8E-03	2.3E-03	2.3E-03	4.9E-03	4.8E-03
AVG site [cm ² /s]	1.7E-02	2.7E-03	4.1E-03		3.1E-03		2.3E-03		5.89E-03	5.74E-03
Compression index	1.5	1.6	1.3	8.4E-01	1.1E	1.1	1.2	9.69E-01	1.2	0.2

evaluation of the coefficient of consolidation. By identifying the initial, primary, and secondary consolidation, which determines the time of 50% consolidation, the coefficient of consolidation (c_v) was calculated as

$$c_v = 0.197 \times \frac{(h)^2}{t_{50\%}} = \frac{k}{m_v \gamma_w} \quad (1)$$

with h , the height of the sample at 50% consolidation; $t_{50\%}$, time of 50% consolidation; k , the hydraulic conductivity; m_v , the coefficient of volume compressibility; and γ_w , the specific unit weight of water.

The compression index (C_c) is the slope of the differences of the void ratio and the differences of the effective stress

$$C_c = \frac{\Delta e}{\Delta \log \sigma'} \quad (2)$$

with e , the void ratio, and δ' , the effective vertical stress.

Kinematic free fall penetration tests

In contrast to free fall piezocone tests (*FFCPTu*) like those with the MARUM SUE (Stegmann et al. 2006), STING (Mulhearn 2002), or even standard *CPTus* (Lunne et al. 2002), kinematic free fall penetrometers do not measure cone resistance (q_c) and side friction (f_s) directly but calculate them from acceleration data (Stark 2011; Stephan 2015). NIMROD was combined with the geometrical analysis approach of Roskoden et al. (2018) to estimate the resistance forces of the mud flat and mangrove forest. The kinematic free fall penetrometer NIMROD (Fig. 2) records pressure continuously as well as a wide range of high-accuracy acceleration data (Stark 2011). The vertical accelerometer sensors are in the ranges of $\pm 1.7g$, $\pm 18g$, $\pm 35g$, $\pm 70g$, and $\pm 250g$. In addition, a dual axis accelerometer is used to determine tilt. Logger sampling rate is at 1 kHz. The pressure transducer is used to measure pore water and hydrostatic pressure up to 200 m water depth. NIMROD's weight is approximately 13.5 kg, measuring 81 cm in total length and consists of a 25-cm tail, 46-cm pressure housing, and 10-cm-long cone. Cone diameter is 11 cm; the resulting cone area is 95 cm².

NIMROD was deployed along a transect of ~ 2.25 km length (see Fig. 1, black line marked C). The transect was located at the centre of the forest (and was orientated perpendicular to the shoreline), ~ 3.6 km east of the Waitakaruru River and ~ 5 km west from the Piako River. The transect was divided into two sections:

1. An outer section, which was sampled from a boat (called boat section), extending from the fringe seaward (location names B1 to B25)
2. An inner section (called mangrove section), which was sampled by foot (location names M1 to M9). This section also starts at the fringe but extends landward into the mangrove forest. Deployment was done with a purpose-built free fall tower (Fig. 2b)

For the boat section, NIMROD was deployed using a winch to ensure a consistent height above sea level (Fig. 2). Along the forest transect, NIMROD was deployed using a purpose-built free fall tower, also ensuring a consistent falling height of ~ 120 cm (measured from the tip to ground level, Fig. 2).

A free fall lance penetrates the soil using gravitational acceleration only. Upon impact, the penetrometer decelerates until the external forces such as friction and resistance at the tip exceed the instrument's kinetic energy.

Penetration depth is governed by falling height and sediment properties; therefore, penetration velocity and soil resistance can be used to determine sediment types (Dayal and Allen 1973; Stark 2011; Stoll et al. 2007). Mulukutla et al. (2011) proposed the following factor of firmness (*FF*) as a measure of sediment type:

$$FF = \frac{a_{\max}}{v_i \times t_p \times g} \quad (3)$$

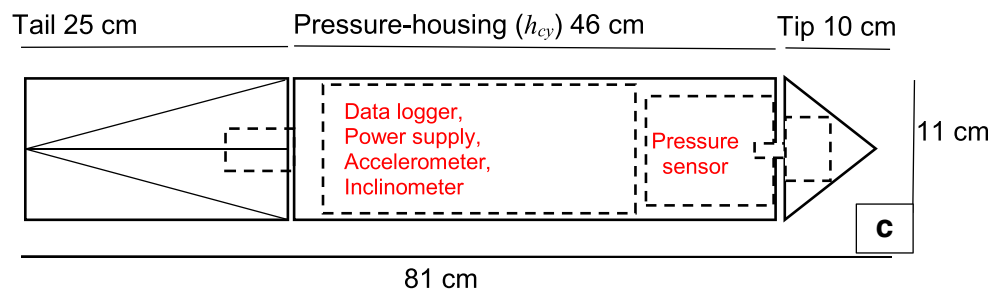
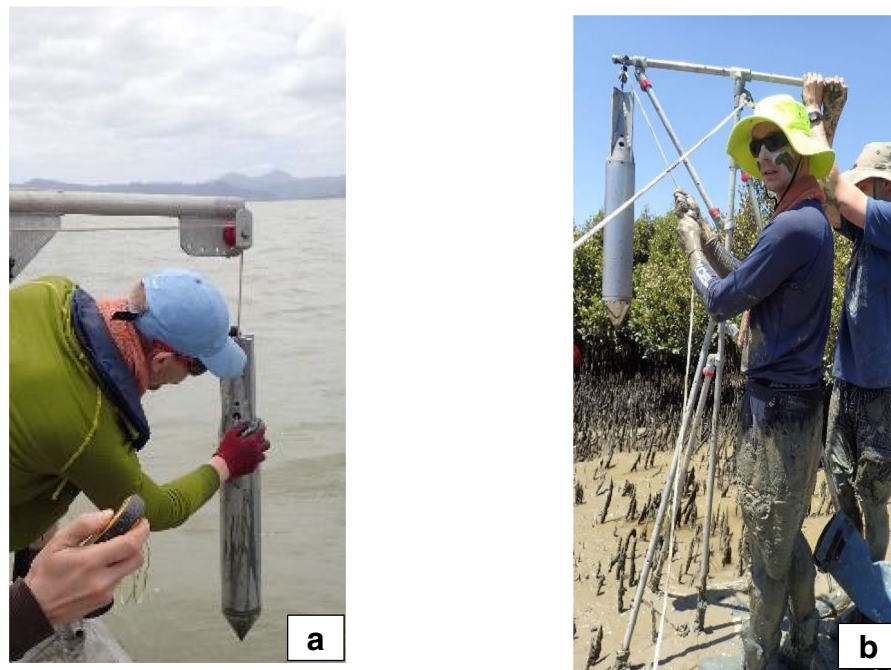
where a_{\max} is the maximum acceleration of the instrument, v_i is the impact velocity, and t_p is the total penetration time and g is the gravitational constant 9.81 m/s². The factor of firmness decreases with an increase of grain size and decreases with the embedded instrument depth.

Further modifications to Eq. (1) were made to connect deceleration records to geotechnical soil characteristics like undrained shear strength (Dayal and Allen 1973; Dayal and Allen 1975; Stark 2011; Steiner 2013; Stoll et al. 2007). For the NIMROD measurements reported here, the original approach from Stark (2011) is used to calculate the quasi-static bearing capacity. The approach was expanded using geometrical considerations to determine quasi-static tip resistance and side friction (Roskoden et al. 2018). In this study, the deceleration and estimated quasi-static bearing capacity, cone resistance and side friction, were utilised to classify the soil and to detect changes between mangrove and non-mangrove areas. Soil samples are used to verify the measurements from NIMROD and correlate geotechnical properties to the penetration data.

Using Newton's second law of motion, the total resistance force (F_t) needed to decelerate NIMROD is:

$$F_t = m \times dec \quad (4)$$

Fig. 2 **a** NIMROD deployed at high tide using a winch on the boat transect; **b** NIMROD deployed using a purpose-built mobile free fall tower, height of the tower 2 m; **c** design print of NIMROD and its dimensions



with m , the mass of NIMROD, and dec , the deceleration. Considering all the possible forces, the total force can be apportioned into

$$F_t = F_q + F_f + F_d + F_b \tag{5}$$

where the force at the tip is $F_q = A_c q_c$ (A_c is the area of the cone and q_c is the cone resistance) and the force at the sides (side resistance) is $F_f = A_s f_s$ (A_s is the area of the side, and f_s is the resistance of the sides). Albatal and Stark (2017) argue that the force at the sides, F_f , the drag force, F_d , and the buoyancy force, F_b , can be neglected due to the limited cone dimension and penetration depth. Hence, Albatal and Stark (2017) do not calculate the cone resistance but the total resistance, which they called the ultimate dynamic bearing capacity

$$q_{ud} = F_t / A_c \tag{6}$$

Roskoden et al. (2018) showed that, especially for cohesive soils, the side friction should not be neglected. Depending on the ratio between the rod and cone area, the influence can make

up to ~40% of the total force (all depending on the geometrical set up of the kinematic free fall probe). Hence, following the argument of Roskoden et al. (2018), Eq. (5) can be reduced to:

$$F_t = F_q + F_f \tag{7}$$

Following Albatal and Stark (2017), we neglect any side friction as long as the height of the submerged cylindrical pressure housing is smaller than 1/3 of the total pressure housing length. After that, side friction cannot be ignored anymore and the total force is divided into tip and side friction resistance forces (F_q and F_f , respectively). The tip force, if the sediment type does not change, should remain constant and can be calculated for a penetration depth smaller than 1/3 of the pressure housing. Afterwards, the tip force can be used as a constant offset value. Thus, any further enhanced total resistance force during penetration can be added to the friction force. If these forces are divided by their respected areas (note: pressure housing area increases with penetration depth, while cone area stays constant), the resulting resistance pressures should remain constant. The resulting dynamic cone

resistance is

$$q_{cd} = F_q/A_c \quad (8)$$

and the dynamic side friction follows

$$f_{sd} = F_f/A_s \quad (9)$$

with the indexes d indicating dynamic values.

For soil characterisation purposes, we also introduce the normalised cone resistance Q_t

$$Q_t = q_n/\sigma'_{v0} \quad (10)$$

with $q_n (= q_t - \delta_{v0})$ being the net cone resistance and $q_t (= q_c + u(1 - a))$ being the pore pressure (u , as measured with NIMROD) corrected cone resistance, δ_{v0} being the total overburden stress, and δ'_{v0} being the vertical effective overburden stress. The normalised friction ratio F_R is

$$F_R = f_s/q_n \quad (11)$$

Possible stratigraphic changes may result for example in an increase of the total resistance force, which will simultaneously cause an enhancement of the frictional resistance. An iterative algorithm can be used to analyse the penetrometer records where these changes are detected and the current tip force is reassessed every time a new layer is identified. A new layer is therefore identified by an atypical change of the side friction pressure (s. Fig. 3).

Dynamic penetration measurements systematically overestimate tip and side resistance forces if compared with standard $CPTu$ measurements (Roskoden et al. 2018). This is called the penetration rate effect (Dayal and Allen 1973, 1975). Attempts have been made to correct for penetration rate effects. For example, Eq. (12) calculates the penetration rate factor (PRF) to correct rate effects on cone resistance:

$$PRF = \frac{q_{cd}}{q_{cst}} = \mu \log_{10} \left(\frac{v}{v_{st}} \right) + 1 \quad (12)$$

with q_{cst} = standard tip resistance, μ = penetration rate factor (different for each considered parameter (Steiner 2013)), v = velocity during penetration, and v_{st} = standard velocity (2 cm/s) (Dayal and Allen 1975; Steiner 2013). Using this correction, the ultimate dynamic bearing capacity can be converted into a quasi-static bearing capacity

$$q_{sbc} = q_{ud}/PRF_{ud} \quad (13)$$

whereas the dynamic tip resistance and side friction result in the quasi-static resistance pressures,

$$q_{cst} = q_{cd}/PRF_{cd} \quad (14)$$

and

$$f_{sst} = f_{sd}/PRF_{sd} \quad (15)$$

where the index st refers to quasi-static parameters.

Penetration velocities and depths (d) are acquired by integrating the deceleration data over time

$$v(t) = \int dec(t) \partial t \quad (16)$$

and

$$d(t) = \iint dec(t) \partial t \quad (17)$$

with t , the time during penetration.

Results

Laboratory work

Grain size distribution

The results for all eight samples are plotted as an average normal and cumulative distribution plot (see Fig. 4). $D_x(10)$ is about 0.8 μm which translates to clay; $D_x(50)$ is around 4.3 μm , which translates to fine silt, and $D_x(90)$ is around 43.9 μm which is fine to coarse silt. In summary, the soil can be interpreted as a clayey medium to coarse silt.

Oedometer testing

Oedometer testing is accomplished by subjecting the sample to known loads (incrementally increased in stages) and measuring the temporal change in vertical deformation after each loading increment. An arbitrary example of the analysis of an oedometer test for the loading stage 250 g or ~ 3 kPa (sample FoT2) is shown in Fig. 5. The deformation is measured using ISO 17892-5 (2017) and then plotted as a semi-logarithmic time plot. A tangent is drawn to the linear part of the curve for the primary and secondary consolidation phases. The cross point (red star) marks the end of the primary consolidation time. $t_{50\%}$ is determined as the midpoint of initial consolidation and end of primary consolidation. With $t_{50\%}$, the coefficient of consolidation is calculated using Eq. (1). The sample heights and diameters were 1.9 and 6.2 cm for each test. Table 1 shows the calculated water and moisture content, dry and bulk density in kg/m^3 , volume of solids and voids in m^3 , the resulting void ratio, the porosity, the averaged coefficient of consolidation in cm^2/s for each sample, and the compression index.

The averaged coefficients of consolidation at each site (M1–M5) show a decreasing gradient from the mud flat to the middle of the forest. A similar gradient can be seen in the compression index. The typical range of the compression index is 0.1 to 10. The higher the compression index, the more

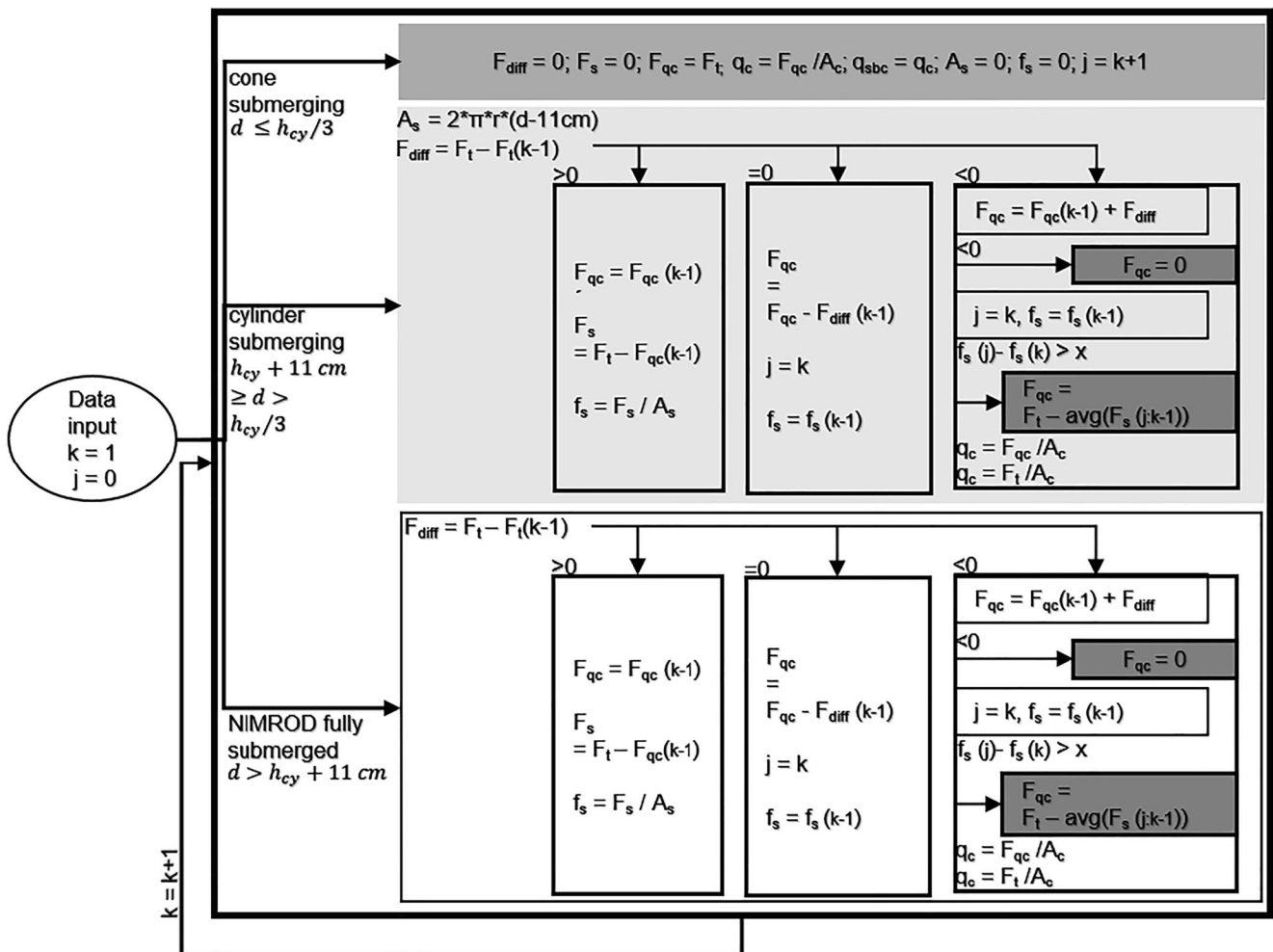


Fig. 3 Schematic of the algorithm implemented to split the total resistance force into the cone resistance and side friction. Glossary k and j are counters for record number, and record number within new layer. d , depth; h_{cy} , cylinder height of NIMROD’s shaft; F , the resistance force; A , area index: $diff$ = difference; t = total; s = side; q_c =

cone resistance; q_{sbc} , quasi-static bearing capacity x , regional threshold (here: $1.5 \times$ side friction, can be estimated either using meta data or chosen arbitrary by the analyst). NOTE: specifically, the index number of the variables in the for-loop is always k

compressible the soil. Hence, the compression index follows a linear trend (slope ~ -0.0227) from sample FoT1 to FoT8, showing a reduction in the compression values.

Analysis of acceleration data

The maximum theoretical free fall velocity is predicted to occur at 5 m water depth. Hence, the variations for the impact velocities for the boat section are relatively high due to water depths of less than 5 m. However, the constant falling height used in the measurements along the mangrove section (controlled by the free fall tower) assures similar impact velocities. Figure 6 shows the soil classification for both transect sections after Mulukutla et al. (2011) (compared with the model by the same authors, represented as a red line). The Mulukutla et al. (2011) classification scheme is based on correlation of the factor of

firmness to the embedded normalised depth. The model classifies grain sizes by characterising their different resistance properties. The classifications by Mulukutla et al. (2011) range from ‘Coarse Silt or softer sediments’ to ‘Medium, Fine, or Very Fine Sand’. The Firth of Thames data plot slightly above the model line. The data shows a transition from ‘Coarse Silt or other soft Sediments’ to ‘Very Coarse Silt’ from the boat transect section to the mangroves section. In both sections, there is a slope showing an increase in the factor of firmness and decrease in embedded normalised depth. The factor of firmness increases with enhancing mangrove density.

After the geometrical-algorithm (Fig. 3) was applied to the acceleration data, the tip resistance and sleeve friction could be plotted for the mud plane and mangrove forest (Fig. 7). Displayed are the rate-corrected variations of quasi-static bearing capacity (also called total resistance pressure) and cone resistance (Fig. 7A and C) with depth. In the case of the

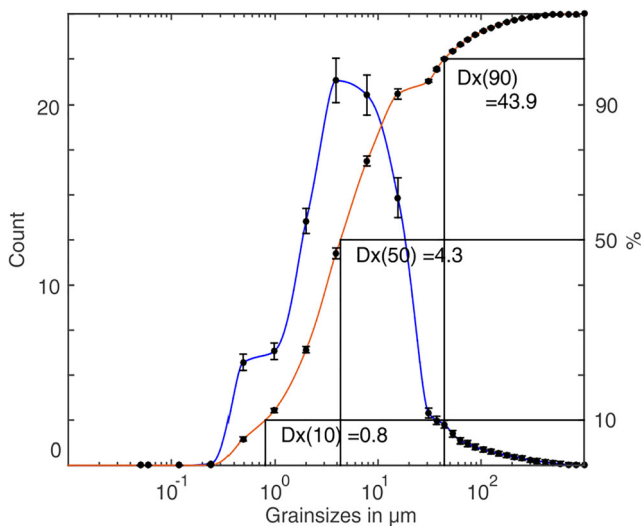


Fig. 4 Grainsize analysis of the samples FoT1 to FoT2 at location M1 to M4. Singular grainsize analysis do not differ in curve form; therefore, an average grainsize was calculated and the single grainsizes were used to calculate standard deviations, which were used to calculate the error bars

mangrove data, there is almost no difference between the tip resistance and the quasi-static bearing capacity (Fig. 7A). In the case of the mud flat data, a clear difference is visible between the quasi-static bearing capacity and the cone resistance (Fig. 7C). While the quasi-static bearing capacity increases with depth up to 150 kPa, the tip resistance stays constant at ~ 80 kPa. The change in the quasi-static bearing capacity is due to the enlargement of the submerging pressure housing area. The tip resistance would only change if the sediment type changed as well. In comparison with the mangrove data, the tip resistance of the mud flat data is 2.5 times less dominant (Fig. 7A and C). The rate-corrected side friction increases at first in the upper 2 cm (Fig. 7B and C), but fluctuates between

0.5 and 1.5 kPa in the case of the mangrove data (panel B). In the case of the mud flat, the side friction increases slightly with depth and levels around 5 kPa and the side friction (Fig. 7D) is around 5 times higher than with the mangrove data (Fig. 7B).

The global soil classification chart from Robertson et al. (1992) can be used to determine the general geotechnical soil type. The classification is not based on grain size but rather on behaviour types. Therefore, the chart illustrates where a given sediment plots in comparison with the background data of the classification scheme. The sediment types are described in Table 2.

Normally, kinematic penetration data cannot be used for these classification schemes due to the lack of friction information. However, after applying the geometrical algorithms after Roskoden et al. (2018) (s. Figure 3) to divide the total resistance values in to tip and side resistance forces, an application of Robertson et al. (1992) can be attempted for the first time. For each NIMROD deployment, an average geotechnical soil type is calculated using the tip resistance and side friction. The data are plotted in their normalised form in Robertson et al. (1992)'s classification chart (Fig. 8a). The colour scheme in Fig. 8 represents the distance to the most landward data point (M9) in the mangrove section measurements. Figure 8a shows the classification chart itself, while Fig. 8b shows the same data as in the classification. The sediments collected along the boat section were identified as 68% soil behaviour type 3 (Clays—silty clay and clay) and 32% as type 4 (Silt mixtures, clayey silt to silty clay). Eighty-eight percent of soil type 4 is within 100 m distance to the mangroves mud flat interface.

The sediments on the mangrove section are characterised as 11% of soil type 3, 4, and 5 (silty sand to sandy silt),

Fig. 5 Display of the oedometer FoT2 stage 250 g or ~ 3 kPa. Vertical deformation is plotted against the $\log(t)$. Red values are estimated using the Casagrande method to determine the initial consolidation, which marks the beginning of the primary consolidation and the end of the primary consolidation. Start and end points of the primary consolidation phase are utilised to estimate $t_{50\%}$. We used sample FoT2 for this example. Note: Even if the vertical load changes, the ratio of hydraulic conductivity and coefficient of volume change, from Eq. (1), does not change (Terzaghi et al. 1996). Therefore, the coefficient of consolidation can be averaged for all loading steps (s. Table 1)

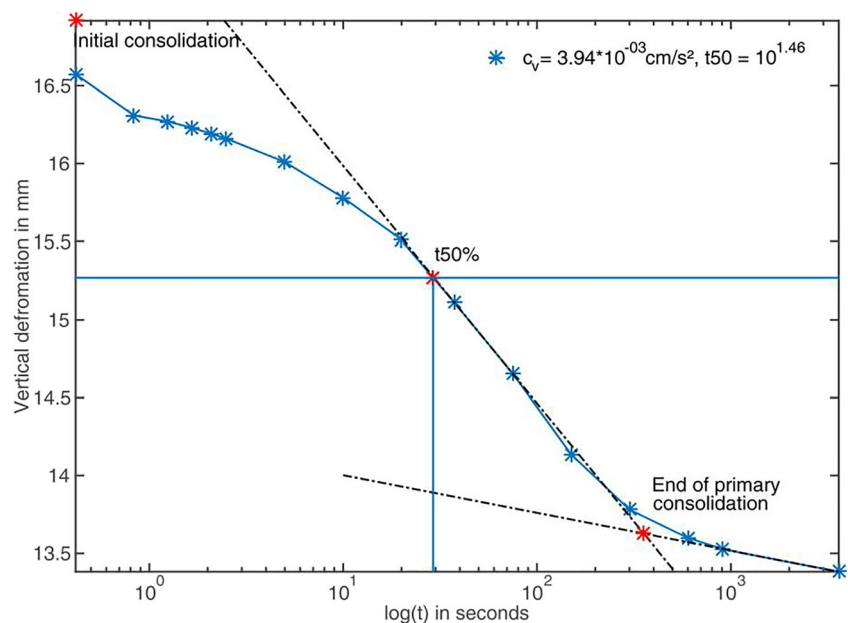


Fig. 6 Classification after Mulukutla et al. 2011. The two different sections of the transect are classified by two different fields. Data are assigned indicative letters **m** for mangrove and **b** for boat transect. Both sections show an increase in FF and a decrease in the embedded depth with a dependency on the mangrove density

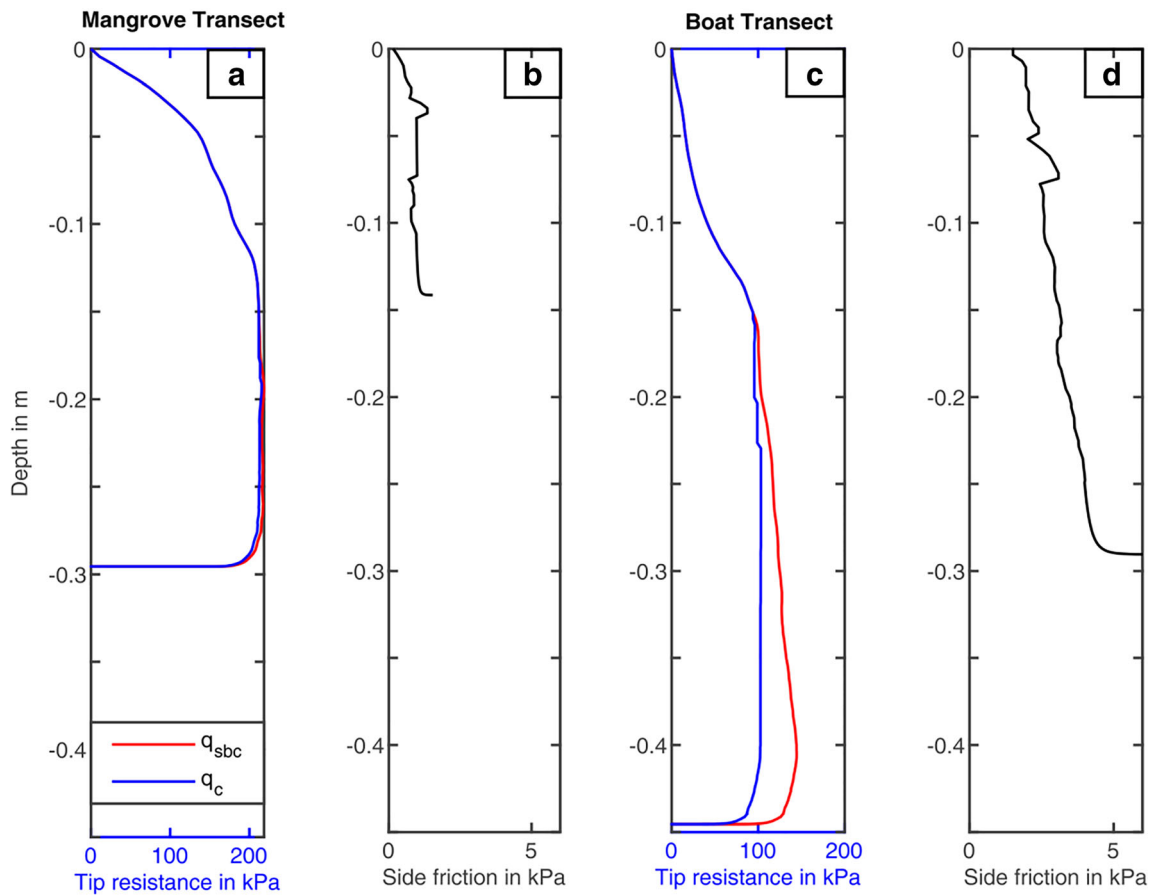
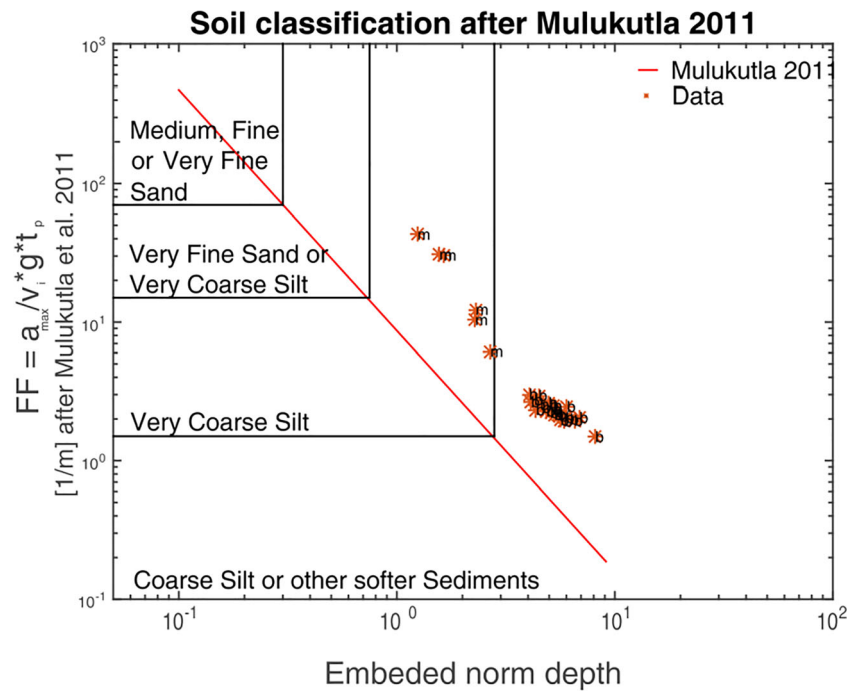


Fig. 7 Comparing mangrove (M4, 80 m away from the mangrove-mud flat interface) with mud flat data (B2, ~72 m away from the interface). Penetration depth in the mud flat is much higher and the side friction is 5 times more dominant. As a consequence, the difference between the tip

resistance and the quasi-static bearing capacity (or total resistance) does not differ much. However, the quasi-static bearing capacity is two times higher at a comparable penetration depth (30 cm)

Table 2 Soil behaviour types after Robertson et al. (1992)

Zone	Soil behaviour type	Classification index (I_c)
1	Sensitive, fine grained	N/A
2	Organic soils—peats	> 3.60
3	Clays—silty clay to clay	2.95–3.60
4	Silt mixtures—clayey silt to silty clay	2.60–2.95
5	Sand mixtures—silty sand to sandy silt	2.05–2.60
6	Sands—clean sand to silty sand	1.31–2.05
7	Gravelly sand to dense sand	< 1.31
8	Very stiff sand to clayey sand*	N/A
9	Very stiff, fine grained*	N/A

* Heavily over-consolidated or cemented

respectively. However, 55% of the data are identified as soil type 6 (clean sand to silty sandy silt). The last 11% do not plot on the chart because the penetration depth was not deep enough to produce the side friction data. Nevertheless, a direct correlation between mangrove density and soil behaviour type is evident for both transects. Note that the sediment grain size did not change substantially over the study transect indicating that all changes in the soil behaviour type are due to the presence of mangroves.

In order to identify the influence of the mangroves on the soil, we compared the quasi-static bearing capacity in the mangrove forest with the coefficient of consolidation from the eight samples (s. Fig. 9c). Note that information on vegetation characteristics (taken from Montgomery et al. 2018)

was not available for all sampling sites and was interpolated for Fig. 9b.

Figure 9a displays the normalised density of mangrove trees and pneumatophores (aerial roots) per m^2 , correlated with the distance to the mangrove-mud flat interface (interface at distance 0 m, negative distance values refer to distances outside the mangrove forest seaward). The linear correlation is used to calculate the normalised density to the locations where data points are collected in this study. The normalised tree density is then correlated to the quasi-static bearing capacity and the coefficient of consolidation (Fig. 8b). The tree density data only explains 39% of the variability in the coefficient of consolidation, whereas the tree density explains 57% of the quasi-static bearing capacity variability. Figure 8c shows the correlation between the coefficient of consolidation (y -axis) and the quasi-bearing capacity (x -axis) in a double logarithmic plot. With an increase of quasi-static bearing capacity, the coefficient of consolidation decreases. The relationship is best characterised by a power law relationship, which explains 75% of the variability. A decrease in the coefficient of consolidation indicates a decrease in the rate at which the soil undergoes consolidation. Softer and more saturated soils have a high coefficient of consolidation, while firmer and less saturated soils have a lower coefficient of consolidation. The change in magnitude for the coefficient of consolidation at normalised tree densities of 5% is clearly shown (compare panels b and c). This indicates that the threshold, which changes the coefficient of consolidation, is 5% of mangrove tree population per m^2 (normalised). In other words, a

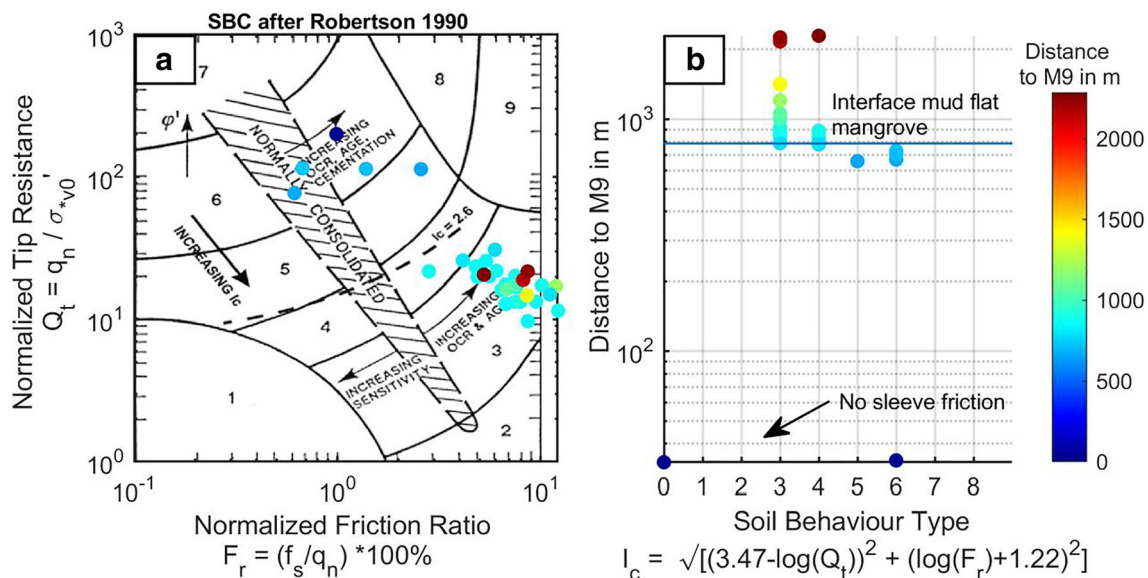
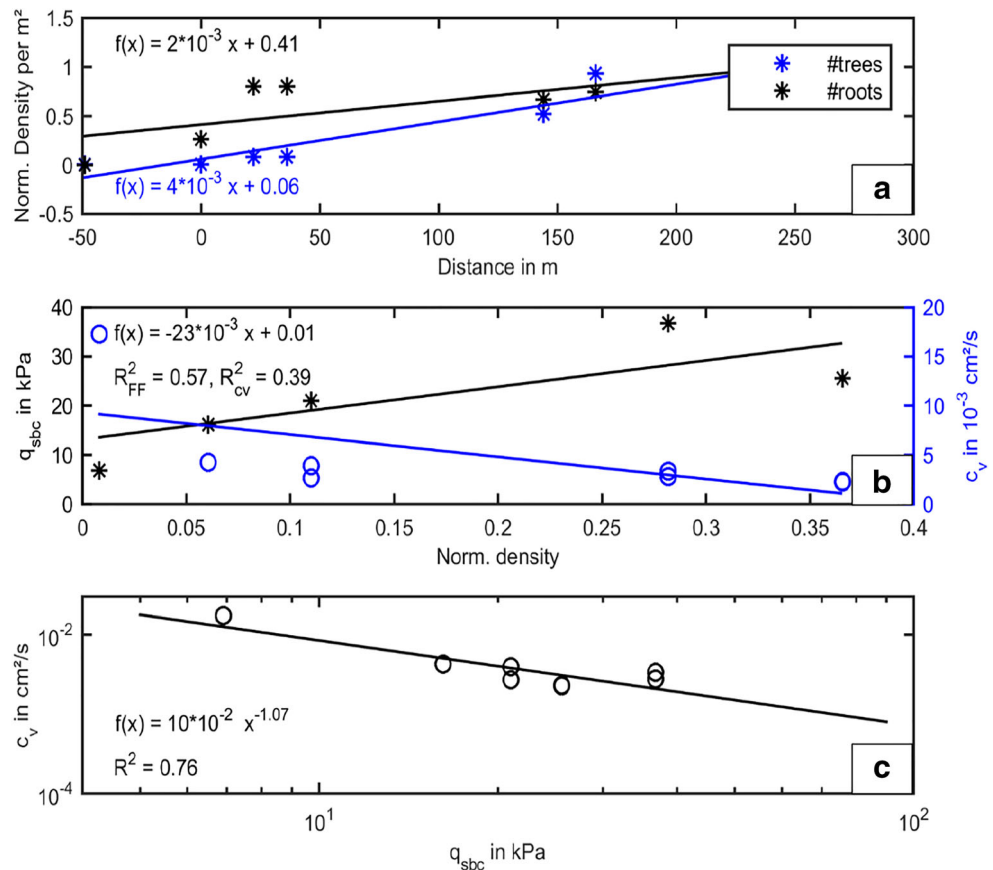


Fig. 8 Soil behaviour chart after Robertson (1990). **a** Soil behaviour fields plotted as a function of the normalised friction ratio and tip resistance. **b** Soil behaviour types (SBT) calculated via the I_c value (formula in figure) on the x -axis plotted versus the distance (M9, ~ 800 m south of the interface of the mud flat and mangrove forest

marked with an arrow, ‘No sleeve friction’ is closest to the land. Its distance is set to 0; hence, distance increases seaward). Colour in data points (panel b) represents distance and follow the same colour coding as in panel a

Fig. 9 Correlation plots. **a** Linear correlation of the normalised number of trees/ aerial roots per m² and position, data from Montgomery et al. (2018). **b** Correlation of the quasi-static bearing capacity and coefficient of consolidation to the normalised tree density (density calculated using the correlation of panel **a**). **c** The double logarithmic plot of the coefficient of consolidation to the quasi-static bearing capacity showing a power law correlation with $R^2 = 0.76$. Note: M3 and M5 have each one q_{sbc} and two c_v values (because M3–M5 have each two samples)



mangrove cover of 500 cm² per m² is necessary to change consolidation properties of the soil from soft and highly saturated (so soil behaviour type 3 and 4 after Robertson’s classification chart (1992)) to firm and low saturation.

Note: Pore pressure measurements were not utilised for this field investigation, since the filter stone was clogged after the first measurements. For further investigation in any mangrove forest during low tide, we suggest to use silicon oil for filter saturation instead of water. Furthermore, a portable high-pressure cleaner would be of use.

Discussion

Eight in situ samples were processed for grain size and subjected to oedometer tests, which evaluated the consolidation properties and trends along a transect of measurements that covers mangrove and mudflat areas. The trend analysis emphasises differences in the consolidation behaviour from the mud flat compared with the mangrove forest. In addition, different soil classification schemes were applied to the acceleration data from the Firth of Thames. The technique of Roskoden et al. (2018) was used to differentiate between total resistance, tip resistance, and side friction. This allowed the first application of the Robertson (1990) soil

classification chart for a dynamic free fall penetrometer. Grain size analysis from sediment samples was used to ground-truth the penetrometer data.

Consolidation due to mangroves roots

A change in the coefficient of consolidation normally depends on the grain size distribution, if sediment types with the same consolidation history are compared. Since no change in the sediment properties was confirmed by the grain size analyses, we can directly link the alteration of the coefficient of consolidation to the density of the mangrove trees. Mangroves reduce the coefficient of consolidation and, by doing so, create a more consolidated soil. We believe that the main mechanisms behind this consolidation are the dewatering of the sediment by mangrove roots (from here on called ‘osmotic-consolidation’), which is governed by the depth level of the roots (as a function of tree height), the root density and types of roots, and the physical structures of the roots themselves, which provide an additional resistance on the penetrometer. Several studies have shown that soils in un-impacted mangrove sites have greater shear strength than sites where the roots and trees have been damaged (e.g. by hurricanes or clear-cutting, reviewed in McIvor et al. (2013)), which they attribute to the binding of surface soil by root structures. Mangrove soils are

also known to shrink and expand in response to osmotic pressure caused by the mangrove roots (Cahoon et al. 2011; Gilman et al. 2008). In addition to these two mechanisms, the weight of the mangrove trees themselves would cause an increase in the overburden weight, which would consolidate the sediments within the forest. Finally, mangroves also occur over a defined range of inundation regimes, and so an increase in mangrove abundance is also associated with an increase in the average duration of exposure to air, which in turn causes an increase in evaporation and consolidation in sediments (Fiot and Gratiot 2006).

Our observations of the effect of mangroves on consolidation are also confirmed by a decreasing compression index trend. The higher level of consolidation not only reduces the erosion risk of tidal currents and wind waves but also reduces future consolidation potential. The estimated low coefficient of hydraulic conductivity of ~ 1 cm/a (Swales et al. 2015) in conjunction with the coefficient of consolidation results presented here suggests a low compressibility soil around the mangroves. The sediment input measured at the study site is 25 to 31 mm/a (Swales et al. 2016). The bulk density is 400 to 590 kg/m³ (Swales et al. 2016). These aforementioned facts cause a stress increase of up to 1 to 2.36 kg/a per m². This stress increase per year roughly equals to the first loading step of the oedometer tests. Hence, we can use the final deformation values of the oedometer test (for 3 kPa) to estimate the vertical deformation due to the extra loading of the annual sediment inputs. The vertical deformation due to consolidation is 5.6 mm (mud flat, M1) to 2.4 mm (at the middle of the mangrove forest, M5). With an averaged relative sea level rise extracted from satellite data (1993–2015) of 4.3 mm/a (Swales et al. 2016) added to the consolidation, the vertical change in height could be 6.7 to 9.9 mm/a. This suggests that mangrove-induced consolidation reduces the elevation of a sediment deposit by up to 42% in the Firth of Thames, therefore, playing a significant role in surface elevation change prediction. From a geotechnical point of view, this change in consolidation is due to the mangroves and, considering the high sedimentation rate, this study site is still accreting at a greater rate than SLR. Furthermore, the soil, consolidated by the mangroves, is more resistant to other vertical changes induced by erosion and further self-weight consolidation processes as aforementioned.

Our work shows that mangrove forests are highly influenced by consolidation processes. Hence, SET-measurements need to account for consolidation processes to capture the real sediment surface evaluation.

Analysis of acceleration data and soil classification

Soil classification charts normally identify sediment deposits without the consideration of embedded rocks and/or roots. Evidently, any classification applied to sediment collected in

the mangrove transect section may not identify the ‘real’ (i.e. undisturbed) soil strata. Evidence of that are the grain size analysis of the eight samples, which do not show any changes in the sediment type. As a consequence, all sediments should plot in the same SBT field in Robertson’s chart (Fig. 8), but this was not observed. Given that the ‘warmer’ blue colours in Fig. 8 represent proximity to mangroves (i.e. large root density), this means that roots shift the SBT from 3 to 6 despite the similarity in sediment composition.

The classification scheme based on Mulukutla et al. (2011) is easily programmed and the data analysed quickly. The unique technique to incorporate metadata such as penetration time, acceleration, velocity, and depth is a clear advantage. The analysis should be included in every free fall penetrometer investigation even if tip resistance and side friction are measured directly. However, this approach only provides a bulk estimate for each penetrometer drop, providing no information on the variation of structure with depth, in which case the soil classification reduces to a 2D problem. Depending on the scientific question, this might complicate geotechnical investigations. Therefore, the Mulukutla et al. (2011) soil classification scheme, which is based on the acceleration data alone, cannot be applied on the mangrove transects to identify a change in sediment deposits because it is not possible to control for the effect of the mangroves. However, the classification can still be used in the mud flat area.

An application of the Robertson-chart for kinematic penetrometers has rarely been done before. Therefore, the separation algorithm of Roskoden et al. (2018) is an inimitable approach, which allows further geotechnical analysis for deployments of such dynamic penetrometers. In general, the Robertson (1990) soil classification results provided classes such as ‘Clays-Silty Clay And Clay’, ‘Silt Mixtures Clayey Silt to Silty Clay’ (for the boat section) to ‘Sands—Clean Sand To Silty Sand’ (for the mangrove section), which is similar to the classifications after Mulukutla et al. (2011); see Figs. 6 and 8 above. However, Robertson (1990) argues that his behaviour types do not directly identify grain sizes such as clay, silt, and sand and suggests that his defined behaviour types indicate a certain soil behaviour. So, if a data point plots into the field ‘Sands—Clean Sand to Silty Sand’, this particular soil behaves like a sand. However, it could also be an over-consolidated and cemented silt or a clast-, shell detritus-, or root-bearing clay/silt. Therefore, certain geotechnical properties such as the normalised cone resistance, normalised friction ratio, degree of cementation (precipitation of crystalline structures affecting the effective porosity and permeability), sensitivity (ratio of sediment undrained shear strength undisturbed vs remoulded), age (secondary consolidation processes), and over consolidation ratio (ratio of current total overburden effective stress to former total overburden effective stress) have also been evaluated in Robertson’s

chart. Thus, separating the total resistance force/quasi-static bearing capacity of the dynamic penetrometer into cone resistance and side friction gives us the advantage of identifying how the mangrove soil behaves with respect to a global database. Since we correlated the mangrove density to the location in the forest relative to the fringe and the location to the soil behaviour types, we can see that the soil behaviour type changes with mangrove density. The higher the mangrove density in the soil, the higher the sediment behaviour type number. A change from soil behaviour type 3, 4 to 5, 6 suggests a much firmer sediment behaviour with possibly higher cementation (due to roots and/or precipitation of organic matter and/or crystalline structure) and/or a higher consolidation ratio (which would represent here, a ratio of the yield stress and the present effective overburden stress).

Conclusion

An estimation of soil resistance forces in and around mangroves was derived from deceleration data using a portable kinematic free fall penetrometer (quasi-bearing capacity, factor of firmness, cone resistance, and side friction). The data was related to grain size (for the mud flat) and to geotechnical properties such as the coefficient of consolidation (mud flat and mangrove forest). The correlations are shown to follow a power-function relationship. Mangroves were shown to have a strong influence on the soils consolidation behaviour, binding the sediments at place.

Concerning our four scientific objectives, we conclude that:

1. A linear trend between the coefficient of consolidation and the mangrove density was found presenting higher consolidated sediments within the mangrove forest interior (Fig. 9a).
2. NIMROD estimated the resistance forces (factor of firmness, total resistance, tip resistance, and side friction) of the mud flat and mangrove forest. The technique developed in the laboratory by Roskoden et al. (2018) to extract tip resistance and side friction from the acceleration data was tested in the field and was successful (Figs. 6, 7, 8, 9). The application of a global soil classification chart for kinematic free fall penetrometer (s. Fig. 8) allowed identification of geotechnical soil behaviour types for the mud flat and the mangrove forest. The availability of mangroves changed or at least mimicked a change in geotechnical bulk properties such as cementation and or a higher consolidation ratio.
3. The resistance forces can be correlated with the regional coefficients of consolidation. The correlation is a power-function in a double logarithmic plot with a $R^2 = 0.76$ (s. Fig. 9c).
4. The trend is used to predict a reduction in the consolidation process due to mangrove density. The cut-off value appeared to be a normalised tree density of 5%. This changes the soil behaviour from soft with high consolidation potential (M1, compression index 1.55; coefficient of consolidation $1.7 \times 10^{-2} \text{ cm}^2/\text{s}$) to firm with reduced consolidation potential (M5, compression index 0.99 coefficient of consolidation 1.7; coefficient of consolidation $2.3 \times 10^{-3} \text{ cm}^2/\text{s}$). If the final deformation values are compared, the consolidation (vertical deformation due to dewatering) is reduced by 45%.

Overall, the approach allowed us to map the geotechnical properties of intertidal sediments in the upper Firth of Thames quickly in 2 days. More data were collected than expected during both transects. A direct connection between the stiffness of the soil and the mangrove tree density was detected and confirms that sediments that have been consolidated due to mangrove presence tend not to consolidate much further, reducing the vertical deformation potential of mangrove forests with increasing forest density. We highly recommend the usage of portable kinematic penetrometers for remote areas like mangrove forests because they allow a quick, easy, and economically feasible data acquisition.

Acknowledgements Dean Sandwell, Nicola Lovett, and Erik Horstman for excellent field help. Marsden contract 14-UOW-011 to fund Karin R. Bryan's time. Andrew Swales for access to the boardwalk. Vicki Moon for laboratory usage. The DFG programme 'Intercoast' for funding the research stay and PhD project of Robert R. Roskoden.

References

- ISO, 2017. International Organization for Standardization Geotechnical investigation and testing - Laboratory testing of soil - Part 5: Incremental loading oedometer test (ISO 17892-5:2017); , Geotechnical investigation and testing–Laboratory
- Albatal A, Stark N (2017) Rapid sediment mapping and in situ geotechnical characterization in challenging aquatic areas. *Limnol Oceanogr Methods* 15:690–705
- Alongi DM (2008) Mangrove forests: resilience, protection from tsunamis, and responses to global climate change. *Estuar Coast Shelf Sci* 76:1–13
- Cahoon DR, Perez BC, Segura BD, Lynch JC (2011) Elevation trends and shrink–swell response of wetland soils to flooding and drying. *Estuar Coast Shelf Sci* 91:463–474
- Casagrande, A., & Fadum, R. E. (1940). Notes on soil testing for engineering purposes. Series No 8, 74 pp
- Dahdouh-Guebas F, Jayatissa LP, Di Nitto D, Bosire JO, Seen DL, Koedam N (2005) How effective were mangroves as a defence against the recent tsunami? *Curr Biol* 15:R443–R447
- Dayal U, Allen JH (1973) Instrumented impact cone penetrometer. *Can Geotech J* 10:397–409
- Dayal U, Allen JH (1975) The effect of penetration rate on the strength of remolded clay and sand samples. *Can Geotech J* 12:336–348
- Fiot J, Gratiot N (2006) Structural effects of tidal exposures on mudflats along the French Guiana coast. *Mar Geol* 228:25–37

- Gilman EL, Ellison J, Duke NC, Field C (2008) Threats to mangroves from climate change and adaptation options: a review. *Aquat Bot* 89: 237–250
- Kathiresan K, Rajendran N (2005) Coastal mangrove forests mitigated tsunami. *Estuar Coast Shelf Sci* 65:601–606
- Lovelock CE, Cahoon DR, Friess DA, Guntenspergen GR, Krauss KW, Reef R, Rogers K, Saunders ML, Sidik F, Swales A (2015) The vulnerability of Indo-Pacific mangrove forests to sea-level rise. *Nature* 526:559–563
- Lunne T, Powell JJM, Robertson PK (2002) Cone penetration testing in geotechnical practice. Taylor & Francis
- McIvor, A. L., Spencer, T., Möller, I., & Spalding, M. (2013). The response of mangrove soil surface elevation to sea level rise. *Natural Coastal Protection Series: Report 3*. Cambridge Coastal Research Unit Working Paper 42, 59, **ISSN 2050-7941**.
- Montgomery J, Bryan K, Horstman E, Mullarney J (2018) Attenuation of tides and surges by mangroves: contrasting case studies from New Zealand. *Water* 10:1119
- Morrisey DJ, Swales A, Dittmann S, Morrison MA, Lovelock CE, Beard CM (2010) The ecology and management of temperate mangroves. CRC Press, Boca Raton(USA), pp 43–160
- Mulhearn P (2002) Influences of penetrometer probe tip geometry on bearing strength estimates for mine burial prediction. Defence Science and Technology Organisation, Canberra (AUSTRALIA)
- Mulukutla GK, Huff LC, Melton JS, Baldwin KC, Mayer LA (2011) Sediment identification using free fall penetrometer acceleration-time histories. *Mar Geophys Res* 32:397–411
- Robertson PK (1990) Soil classification using the cone penetration test. *Can Geotech J* 27:151–158
- Robertson P, Sully J, Woeller DJ, Lunne T, Powell J, Gillespie D (1992) Estimating coefficient of consolidation from piezocone tests. *Can Geotech J* 29:539–550
- Roskoden, R., Kopf, A., Mörz, T., & Kreiter, S. (2018). Analysis of acceleration and excess pore pressure data of laboratory impact penetrometer tests in remolded overconsolidated cohesive soils. In *Cone Penetration Testing 2018*, pp. 545–550. CRC Press.
- Sasmito, S. D., Murdiyarso, D., Friess, D. A., & Kurnianto, S. (2016). Can mangroves keep pace with contemporary sea level rise? A global data review. *Wetlands Ecology and Management*, 24(2), 263–278
- Stark N (2011) Geotechnical investigation of sediment remobilization processes using dynamic penetrometers. Universität Bremen, Bremen
- Stegmann, S., Mörz, T., & Kopf, A. (2006). Initial Results of a new Free Fall-Cone Penetrometer (FF-CPT) for geotechnical in situ characterisation of soft marine sediments. *Norwegian Journal of Geology/Norsk Geologisk Forening*, 86(3): 199–208
- Steiner A (2013) Sub-seafloor characterization and stability of submarine slope sediments using dynamic and static piezocone penetrometers. Bremen, Universität Bremen, Diss., 2013
- Stephan S (2015) A rugged marine impact penetrometer for sea floor assessment. Bremen, Universität Bremen, Diss., 2015
- Stoll RD, Sun Y-F, Bitte I (2007) Seafloor properties from penetrometer tests. *IEEE J Ocean Eng* 32:57–63
- Swales A, Bentley SJ Sr, Lovelock CE (2015) Mangrove-forest evolution in a sediment-rich estuarine system: opportunists or agents of geomorphic change? *Earth Surf Process Landf* 40:1672–1687
- Swales A, Denys P, Pickett VI, Lovelock CE (2016) Evaluating deep subsidence in a rapidly-accreting mangrove forest using GPS monitoring of surface-elevation benchmarks and sedimentary records. *Mar Geol* 380:205–218
- Terzaghi K, Peck RB, Mesri G (1996) Soil mechanics in engineering practice. John Wiley & Sons New York, 592 pp
- Zhou Z, van der Wegen M, Jagers B, Coco G (2016) Modelling the role of self-weight consolidation on the morphodynamics of accretional mudflats. *Environ Model Softw* 76:167–181

Publisher's note Springer Nature remains neutral with regard to jurisdictional claims in published maps and institutional affiliations.